P H Y S I C A L   R E V I E W   L E T T E R S

Microstructure of Fragile Metallic Glasses Inferred from Ultrasound-Accelerated Crystallization in Pd-Based Metallic Glasses

T. Ichitsubo,[1,]* E. Matsubara,[1] T. Yamamoto,[2] H. S. Chen,[3] N. Nishiyama,[4] J. Saida,[5] and K. Anazawa[2]

[1]*Department of Materials Science and Engineering, Kyoto University, Kyoto 606-8501, Japan*
[2]*Institute for Materials Research, Tohoku University, Sendai 980-8577, Japan*
[3]*Bell Laboratory, Lucent Technology, New Jersey 08833, USA*
[4]*RIMCOF, R&D Institute of Metals and Composites for Future Industries, Sendai 980-8577, Japan*
[5]*Center for Interdisciplinary Research, Tohoku University, Sendai 980-8578, Japan*
(Received 20 May 2005; published 5 December 2005)

By utilizing ultrasonic annealing at a temperature below (or near) the glass transition temperature T_g, we revealed a microstructural pattern of a partially crystallized Pd-based metallic glass with a high-resolution electron microscopy. On the basis of the observed microstructure, we inferred a plausible microstructural model of fragile metallic glasses composed of strongly bonded regions surrounded by weakly bonded regions (WBRs). The crystallization in WBRs at such a low temperature under the ultrasonic vibrations is caused by accumulation of atomic jumps associated with the β relaxation being resonant with the ultrasonic strains. This microstructural model successfully illustrates a marked increase of elasticity after crystallization with a small density change and a correlation between the fragility of the liquid and the Poisson ratio of the solid.

PACS numbers: 61.43.Bn, 61.43.Fs, 62.20.Dc, 62.40.+i

Structures of vitreous substances are one of the attractive subjects of ongoing research in glass science [1]. In general, glasses fall roughly into two classes, "strong" and "fragile" glass-forming liquids from the viewpoint of deviation from the Arrhenius behavior in the temperature dependence of viscosity $\eta(T)$ [2], and the fragility parameter m is frequently defined as

$$m = \frac{\partial \log \eta(T)}{\partial (T_g/T)} \bigg|_{T=T_g}, \qquad (1)$$

where T_g denotes the glass transition temperature. Glasses possessing m close to 1 (i.e., showing the Arrhenius behavior) are called strong, and ones having a larger m are called fragile (or intermediate in the case of not so large m). Strong glass formers such as SiO_2 and GeO_2 ($m \approx$ 10–20) consist of a network of covalently bonded clusters [3]. The elastic modulus of the glassy state is not so different from that of its crystalline phase; for example, the bulk moduli of fused SiO_2 glass and α quartz are both about 36 GPa [4,5]. In addition, Poisson's ratio of SiO_2 is small (~0.17) in the glassy state. In contrast, fragile glasses are not fully explained, and they exhibit the following intriguing aspects in physical properties: (i) Faster dynamic relaxation, called "β (secondary) relaxation," is frequently observed prior to the dynamic glass transition called "α (primary) relaxation" [6–11]. (ii) The elastic modulus changes drastically, by about 30%–50%, after crystallization, although the mass-density change is only about 1%–2% or less [5,12,13]. (iii) A fragile glass former tends to exhibit a large Poisson's ratio in a glassy state [14]. This trend is true for covalently bonded glasses, although it is not observed in metallic glasses.

How can we understand the above characteristic features of fragile glasses? Substantial metallic glasses belong to fragile or intermediate glass formers [15]. In this work, for fragile Pd-based metallic glasses ($m \approx$ 50–60 [16]), we experimentally studied the β relaxation at megahertz frequencies around T_g and demonstrated that atomic motions (or jumps) associated with the β relaxation are stochastically resonant with the ultrasonic vibrations, which eventually leads to crystallization. By utilizing this ultrasound-accelerated crystallization phenomenon [17,18], we reveal a partially crystallized microstructure of the fragile Pd-based metallic glass with a high-resolution electron microscopy. On the basis of the experimental results, we present a possible microstructural model of fragile metallic glasses and demonstrate that the above-mentioned features (ii) and (iii) are illustrated with this model.

Observations of the β relaxation were reported, for example, in Pd-Cu-Si [7], La-Al-Ni [8–10], and Pd-Ni-Cu-P glasses [11]. The activation energy for the β relaxation is known to be far lower than that for the α relaxation, in which cooperative atomic motions occur with a high activation energy. Hence, while the α relaxation is observed around T_g at a low frequency (~1 Hz), the β relaxation is observed far below T_g at the same frequency [6]. When the measurement frequency is raised, however, the β relaxation will be observed at higher temperatures. Actually, we successfully detected the increase of Q^{-1} at megahertz frequencies around T_g for Pd-based glasses by the electromagnetic acoustic resonance method with a signal generator (RAM-10000, RITEC Inc.); the experimental $Q^{-1}(T)$ curves of a $Pd_{40}Ni_{40}P_{20}$ glass are shown in Fig. 1(a). We need to examine whether the increase in the experimental $Q^{-1}(T)$ curves is indeed associated with the β relaxation.
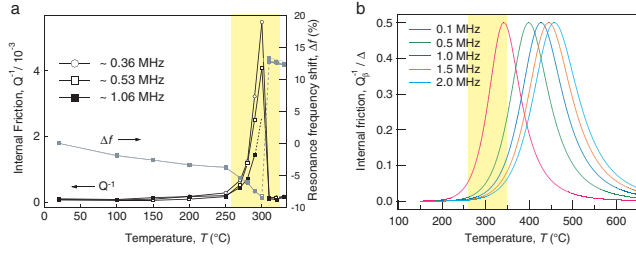
FIG. 1 (color). High-frequency internal friction as a function of temperature for β relaxation in Pd-based metallic glasses. (a) Temperature dependence of high-frequency internal friction measured for $Pd_{40}Ni_{40}P_{20}$ metallic glass ($T_g \approx 300\,°C$). Shear vibration modes were used for the internal-friction measurements, and the rate of temperature scan was about $1\,°C/\min$. The resonance-frequency shifts Δf are also displayed for reference. The sudden drop of Q^{-1} and marked increase in Δf near T_g are caused by abrupt crystallization. (b) Q_{β}^{-1}-T curves calculated using Eq. (2) with $\Delta E \sim 1.0$ eV and $\tau_0 \sim 1.0 \times 10^{-14}$ s taken from the literature [11].

Then the $Q_{\beta}^{-1}(T)$ curves are evaluated in the present frequencies from $\Delta E \sim 1.0$ eV and $\tau_0 \sim 1.0 \times 10^{-14}$ s, which were obtained by the low-frequency (~ 1 Hz) internal-friction measurement for a Pd-Ni-Cu-P glass by Pelletier *et al.* [11]. The internal friction Q_{β}^{-1} caused by the β relaxation process is expressed by the Debye function [7]:

$$\frac{Q_{\beta}^{-1}}{\Delta} = \frac{\omega\tau_0 \exp(\Delta E/kT)}{1 + [\omega\tau_0 \exp(\Delta E/kT)]^2}, \qquad (2)$$

where Δ is the relaxation strength, $\omega(= 2\pi f)$ is the angular frequency (f is the frequency of the oscillator), and $\tau_0 \exp(\Delta E/kT)(= \tau)$ is the relaxation time per event, τ_0 being the atomic/molecular-scale time, and ΔE is the activation energy of the event; kT has the usual meaning. Using the above values by Pelletier with Eq. (2), the $Q_{\beta}^{-1}(T)$ curves were calculated for Pd-based metallic glasses; the results are shown in Fig. 1(b). It is found that the β relaxation is observed around T_g at megahertz frequencies. The experimental temperature dependence of Q^{-1} at various megahertz frequencies around T_g is well reproduced in the calculated profiles of Fig. 1(b). Thus, in the case of Pd-based metallic glasses, the β relaxation which is observed far below T_g at low frequencies is observed at a temperature around or higher than T_g at megahertz frequencies.

The peak shape of the $Q^{-1}(T)$ experimental curves is lambda type and quite different from the calculated Lorentzian-type curves. Notice that the $Q^{-1}(T)$ curves in Fig. 1(a) represent tails that are terminated before reaching the maxima of the peaks. Namely, the Lorentzian-type $Q^{-1}(T)$ curves suddenly fall above T_g (concurrently, the resonance frequencies increase markedly by about 20%, indicating an approximately 40% increase of the shear modulus); the sudden drop of $Q^{-1}(T)$ is attributed to the

abrupt crystallization around T_g. The increase of internal friction indicates that a periodic external stress or strain is stochastically resonant with atomic motions associated with the β relaxation. In such a situation, atomic jumps will become different from ordinary ones; that is, atoms will move into more stable potential sites due to the periodic external stress. It is considered that repetition of such irregular jumps gradually changes the energy landscape and eventually causes crystallization.

By utilizing this ultrasonic annealing (ultrasound-accelerated crystallization phenomenon), we can expose the structural pattern of the Pd-based metallic glasses. Under ultrasonic vibrations (~ 0.35 MHz), $Pd_{42.5}Ni_{7.5}Cu_{30}P_{20}$ glass was found to be fully crystallized within only 18 h at $290\,°C$ ($\leq T_g \approx 300\,°C$). Incidentally, crystallization was negligible when the samples were annealed without ultrasonic vibrations for 75 h at this temperature. In order to obtain a mixture consisting of mainly amorphous regions with a small amount of crystallized regions, a glass sample was annealed at $290\,°C$ for a shorter duration, 10 h, with ultrasonic vibrations of about 0.35 MHz. Figure 2 shows the high-resolution electron microscopy (HREM) image. We can see that the amorphous regions are surrounded by crystallized walls that show the lattice-fringe contrast. This microstructure of the partially crystallized sample is considerably different from a typical microstructure commonly observed [19], in which isolated crystals are formed in the amorphous matrix.

The crystallization by the ultrasonic annealing (below T_g) is strongly related with the β relaxation, and, therefore, by noting the crystallized regions, we can prefigure the intrinsically mobile or soft regions in the amorphous matrix. From this viewpoint, we infer a plausible microstructural model shown in Fig. 3, in which the glassy solid is
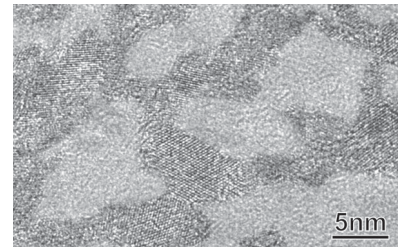

FIG. 2. Typical HREM image of $Pd_{42.5}Ni_{7.5}Cu_{30}P_{20}$ metallic glass after annealing at $290\,°C$ (below or near T_g) for 10 h under ultrasonic vibrations of 0.35 MHz. The remaining amorphous fraction was estimated to be about 80% from the crystallization heat measured by differential scanning calorimetry. It can be clearly recognized that the amorphous domains are surrounded by crystallized walls that show lattice fringes. Ultrasonic vibrations are considered to accelerate crystallization of WBRs via β relaxation. The crystallized walls would be thin if annealing time is shortened. The sample for HREM was prepared by ion milling with cooling using liquid N_2 to prevent crystallization due to ion irradiation. For the sake of conspicuity of the boundaries, the amorphous-like regions are colored grey.

composed of strongly bonded regions (SBRs) and weakly bonded regions (WBRs). This microstructural model is visually similar to some theoretical structural models, such as Stillinger's model [20], the modified continuous random network model by Greaves [21], the island of mobility model by Johari [22], the entropy and density fluctuation model by Ediger [23], and the concept of cooperatively rearranging region and its correlation length by Donth [24], or qualitatively similar to the concept of inhomogeneous internal-stress distribution [25,26]. The feature of the present model is that SBRs are surrounded by WBRs, where the atomic motions are relatively fast and the β relaxation takes place.

In what follows, let us examine the characteristic features (ii) and (iii) aforementioned with this microstructural model. First, we consider the reason why the elastic modulus changes drastically upon crystallization with a very small change in the mass density. Here, by using the effective-mean-field (EMF) theory [27], we calculate macroscopic elastic constants for the model in Fig. 3(b) and consider how they change with fractions of WBR and SBR. For the sake of simplicity, both WBRs and SBRs are assumed to be elastically isotropic. The elastic constants of WBR are considered to be soft and to have a large Poisson's ratio. For SBR, we consider two typical cases: (a) Poisson's ratios in SBRs are fairly large and close to those in WBRs (corresponding to metallic glasses), and (b) Poisson's ratios in SBR are far smaller than those in WBRs (standing for oxide or polymer glasses containing network modifiers). Then two sets of elastic constants are assigned for SBRs, referring to the literature [5,12]. The macroscopic elastic constants of the above mixtures are calculated using the EMF theory under the condition of spherical inclusions. (As far as the magnitude of the elastic constants used in the calculations is retained, even when

the shape of the inclusions is changed, the qualitative argument is unchanged.)

Figures 4(a) and 4(b) correspond to the results for the above two cases. The left graphs show the macroscopic modulus $\bar{c}_{ij}$ in the case where SBRs are embedded in the WBR matrix (i.e., for the model in Fig. 3), and the right ones are for the opposite case (i.e., the microstructural topology is reversed). We find that, when a very small amount of WBR exists in the former case, $\bar{c}_{ij}$ markedly decreases (about 40% decrease with only 3% WBR). However, when a small number of WBRs are embedded in the SBR matrix, only almost linear variation is seen. Therefore, the structure in which SBRs are embedded in WBR is appropriate for expressing the drastic change in the elastic constants upon crystallization. Then a large mass-density change in WBR is acceptable, because the amount of WBR is quite small and, therefore, the overall density of the glass substance will appear to be substantially unchanged.
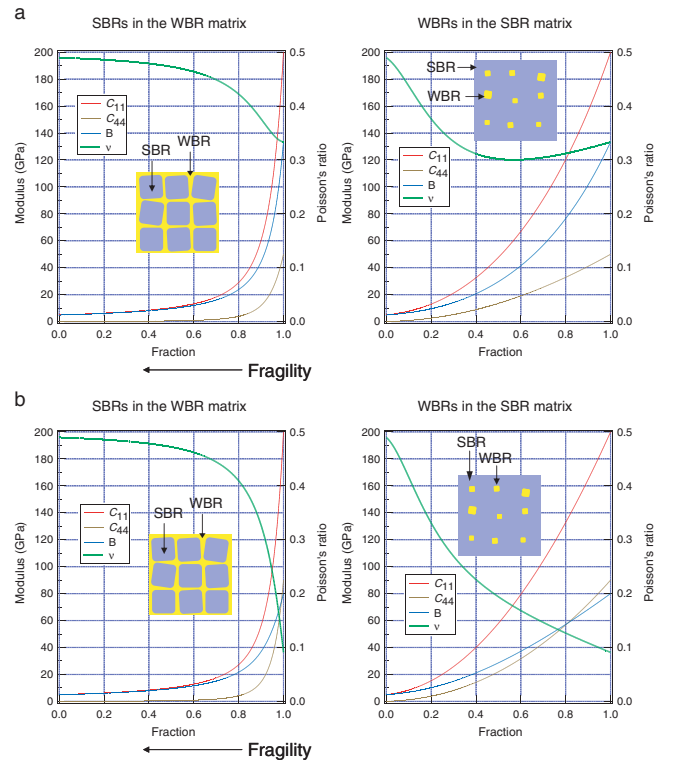
FIG. 4 (color).   Macroscopic elastic constants of glasses composed of SBRs and WBRs as a function of the volume fraction of SBRs. The elastic constants of WBRs are $c_{11} = 5$ GPa and Poisson's ratio ν is 0.49. (a) Poisson's ratio in SBR is large compared with that in WBR. The elastic constants in SBRs are $c_{11} = 200$ GPa and $\nu = 0.33$. (b) Poisson's ratios in SBRs and WBRs differ greatly. The elastic constants in SBRs are $c_{11} = 200$ GPa and $\nu = 0.09$. In the present calculations, although the elastic constants are arbitrarily chosen for SBRs and WBRs, as long as the magnitude relationship is maintained, changing the values does not affect the qualitative discussion.
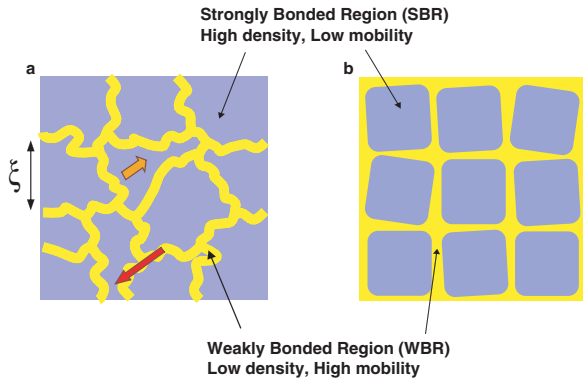

FIG. 3 (color).   (a) Microstructural model of fragile metallic glasses inferred on the basis of the microstructure of the ultrasonic-annealed sample (Fig. 2). (b) Simplified model for computing the macroscopic elastic moduli. In this model, the glassy substances are separated into two parts: SBRs and WBRs. Atomic mobility in WBRs is higher than that in SBRs (the long and short arrows denote the atomic mobility). The symbol ξ represents the characteristic length.

Next we try to apply the model to the correlation between elasticity and fragility recently found by Novikov and Sokolov [14]. In general, the viscosity depends on the material itself. To a certain degree, however, the fragility can also be discussed in terms of the microstructure. According to Cohen-Grest's free-volume theory [28] or Egami's local topological instability theory [29,30], WBR becomes unstable as a solid at a lower temperature (i.e., at a glass transition temperature T_g) than SBR, because the local bulk modulus of WBR is lower than that of SBR (the melting temperature is empirically proportional to the bulk modulus). Namely, it is reasonable to consider that WBRs first transform from solidlike to liquidlike near T_g. According to the fragility parameter defined by Eq. (1), the viscosity $\eta(T)$ decreases steeply just above T_g when m is large. In this model, WBR becomes liquidlike around T_g (SBR remains still solidlike), so that a glass containing a larger amount of WBR in the frozen state will exhibit a larger m. Then we see another interesting feature in the left figure in Fig. 4(b): As the fraction of SBR decreases, only a few percent from 1, the Poisson's ratio of the glass increases steeply. Thus, this structural model explains well the intriguing findings that glasses having a large Poisson's ratio exhibit high fragility. It is noted here that the present demonstration is based only on the microstructural insight, not based on the bonding forms (e.g., covalent, ionic, or metallic bonds), but the elasticity-fragility correlation obtained by Novikov and Sokolov [14] can be understood with the present model in part.

In conclusion, we revealed the microstructure of a partially crystallized Pd-based metallic glass by utilizing the ultrasonic annealing, where atomic motions associated with the β relaxation are stochastically resonant with the ultrasonic vibrations, and, on the basis of the present experimental results (Figs. 1 and 2), we inferred a plausible microstructural model (Fig. 3) of fragile metallic glasses. The present microstructural model is consistent with the heterogeneous-structural models previously proposed by other researchers [20–26]. With the model, we can understand the characteristic features (on elasticity or fragility) observed for fragile glasses. Thus, the deduced microstructural model is sufficient for explaining well the experimental data, but the interpretation of the data may not be unique. To obtain more direct evidence of the structure is a future challenging subject. Further investigation will provide accurate information on the typical domain size ξ in such an inhomogeneous microstructure of the crystallized state, which enables us to compare with the correlation length based on the statistical thermodynamics by Stillinger [20] or the characteristic length associated with the cooperatively rearranging regions by Donth [24].

*Electronic mail: tichi@mtl.kyoto-u.ac.jp

[1] D. B. Miracle, Nat. Mater. **3**, 697 (2004).
[2] C. A. Angell, J. Non-Cryst. Solids **73**, 1 (1985); C. A. Angel, K. L. Ngai, G. B. McKenna, and S. W. Martin., J. Appl. Phys. **88**, 3113 (2000).
[3] S. R. Elliott, *Physics of Amorphous Materials* (Longman, London and New York, 1984).
[4] Q. Wang, G. A. Saunders, E. F. Lambson, P. Tschaufeser, S. C. Parker, and B. J. James, Phys. Rev. B **45**, 10 242 (1992).
[5] Bo Zhang, R. J. Wang, D. Q. Zhao, M. X. Pan, and W. H. Wang, Phys. Rev. B **70**, 224208 (2004).
[6] P. G. Debenedetti and F. H. Stillinger, Nature (London) **410**, 259 (2001).
[7] H. S. Chen and N. Morito, J. Non-Cryst. Solids **72**, 287 (1985).
[8] H. Okumura, H. S. Chen, A. Inoue, and T. Masumoto, Jpn. J. Appl. Phys. **30**, 2553 (1991).
[9] H. Okumura, H. S. Chen, A. Inoue, and T. Masumoto, J. Non-Cryst. Solids **130**, 304 (1991).
[10] H. Okumura, H. S. Chen, A. Inoue, and T. Masumoto, J. Non-Cryst. Solids **150**, 401 (1992).
[11] J. M. Pelletier, B. Van de Moortèle, and I. R. Lu, Mater. Sci. Eng. A **336**, 190 (2002).
[12] L. M. Wang, W. H. Wang, R. J. Wang, Z. J. Zhan, D. Y. Dai, L. L. Sun, and W. K. Wang, Appl. Phys. Lett. **77**, 1147 (2000).
[13] D. Weaire, M. F. Ashby, J. Logan, and M. J. Weins, Acta Metall. **19**, 779 (1971).
[14] V. N. Novikov and A. P. Sokolov, Nature (London) **431**, 961 (2004).
[15] H. Tanaka, Phys. Rev. Lett. **90**, 055701 (2003).
[16] Y. Kawamura, T. Nakamura, H. Kato, H. Mano, and A. Inoue, Mater. Sci. Eng. A **304–306**, 674 (2001).
[17] T. Ichitsubo, E. Matsubara, S. Kai, and M. Hirao, Acta Mater. **52**, 423 (2004).
[18] T. Ichitsubo, S. Kai, H. Ogi, M. Hirao, and K. Tanaka, Scr. Mater. **49**, 267 (2003).
[19] M. Wollgarten, S. Mechler, E. Davidov, N. Wanderka, and M.-P. Macht, Intermetallics **12**, 1251 (2004).
[20] F. H. Stillinger, J. Chem. Phys. **89**, 6461 (1988).
[21] G. N. Greaves, J. Non-Cryst. Solids **71**, 203 (1985).
[22] G. P. Johari and M. Goldstein, J. Chem. Phys. **53**, 2372 (1970).
[23] M. D. Ediger, J. Non-Cryst. Solids **235–237**, 10 (1998).
[24] E. Donth, J. Non-Cryst. Solids **53**, 325 (1982); E. Hempel, G. Hempel, A. Hensel, C. Schick, and E. Donth, J. Phys. Chem. B **104**, 2460 (2000).
[25] S. Alexander, Phys. Rep. **296**, 65 (1998).
[26] T. Kustanovich, Y. Rabin, and Z. Olami, Phys. Rev. B **67**, 104206 (2003).
[27] M. Tane and T. Ichitsubo, Appl. Phys. Lett. **85**, 197 (2004).
[28] M. H. Cohen and G. S. Grest, Phys. Rev. B **20**, 1077 (1979).
[29] T. Egami, Mater. Sci. Eng. A **226–228**, 261 (1997).
[30] T. Egami, Mater. Trans., JIM **43**, 510 (2002).